

Cavity-enhanced optical feedback-assisted photo-acoustic spectroscopy with a 10.4 μm external cavity quantum cascade laser

A. Kachanov · S. Koulikov · F. K. Tittel

Received: 12 September 2012/Revised: 13 September 2012/Published online: 23 November 2012
© Springer-Verlag Berlin Heidelberg 2012

Abstract An ultra-sensitive photo-acoustic spectrometer using a 10.4 μm broadly tunable mid-IR external cavity quantum cascade laser (EC-QCL) coupled with optical feedback to an optical power buildup cavity with high reflectivity mirrors was developed and tested. A laser optical power buildup factor of 181 was achieved, which corresponds to an intra-cavity power of 9.6 W at a wavelength of 10.4 μm . With a photo-acoustic resonance cell placed inside the cavity this resulted in the noise-equivalent absorption coefficient of $1.9 \times 10^{-10} \text{ cm}^{-1} \text{ Hz}^{-1/2}$, and a normalized noise-equivalent absorption of $1.1 \times 10^{-11} \text{ cm}^{-1} \text{ W Hz}^{-1/2}$. A novel photo-acoustic signal normalization technique makes the photo-acoustic spectrometer's response immune to changes and drifts in the EC-QCL excitation power, EC-QCL to cavity coupling efficiency and cavity mirrors aging and contamination. An automatic lock of the EC-QCL to the cavity and optical feedback phase optimization permitted long wavelength scans within the entire EC-QCL spectral tuning range.

1 Introduction

Laser photo-acoustic spectroscopy (PAS) is an effective technique for trace gas sensing because it combines high sensitivity and the ruggedness required for field deployable instrumentation [1]. Significant progress has been made in

PAS. Methods of modeling and design of the PAS cells have been developed, which achieved photo-acoustic cells close to optimum. Different designs of resonant PAS cells based upon miniature electret condenser microphones have been reported by several research groups [2–4]. This resulted in similar values of normalized noise-equivalent absorption (NNEA) of $\sim 1 \times 10^{-9} \text{ cm}^{-1} \text{ W Hz}^{-1/2}$ regardless of their different acoustic resonator arrangement, acoustic cell volume and resonant frequency. This raises the question whether these designs reached a fundamental limit due to pressure fluctuations of air in the cell resulting from the Brownian motion of air molecules as suggested by Kreuzer [5]. In 1971, Kreuzer considered that this fundamental limit was not achievable because microphone pre-amplifier noise would dominate the Brownian noise. The technology of miniature low noise electret microphones with an integrated pre-amplifier has led to a fundamental limit dominated by thermal motion of air molecules [6]. In this work the electronic noise contribution of a miniature microphone (Knowles EM-3346) as determined from vacuum measurements was <10 dB below the thermal noise for a microphone with an operating bandwidth from $\sim 30 \text{ Hz}$ to 10 kHz. This may explain the similar detection sensitivity values reported by several groups.

Furthermore, several attempts have been made to replace a traditional microphone with an even better PAS transducer. For example, in Ref. [7] the photo-acoustic pressure was detected by measuring deflection of a micro-mechanical cantilever with a laser interferometer. Using a small PAS cell in a non-acoustic-resonance mode and exploiting the inverse proportionality of the cell response to the excitation frequency the authors reported a sensitivity of $2.8 \times 10^{-10} \text{ cm}^{-1} \text{ W Hz}^{-1/2}$ for CO_2 in N_2 . However, despite a three-time gain in the detection

A. Kachanov · S. Koulikov
LI-COR Biosciences, 3671 Enochs St.,
Santa Clara, CA 95051, USA

F. K. Tittel (✉)
Department of Electrical and Computer Engineering,
Rice University, 6100 Main Street, Houston, TX 77005, USA
e-mail: fkt@rice.edu

sensitivity as compared to the best microphone-based results, such a system is not suitable for its implementation in low-cost, portable field gas analyzers. Another non-microphonic sensor platform known as quartz-enhanced photo-acoustic spectroscopy (QEPAS) [8], offers a low-cost option and small detection volume. QEPAS best detection sensitivity expressed in terms of the NNEA is $6.3 \times 10^{-10} \text{ cm}^{-1} \text{ W Hz}^{-1/2}$ [9].

With a detection sensitivity limited by NNEA of $\sim 10^{-9} \text{ cm}^{-1} \text{ W Hz}^{-1/2}$ and output powers of available commercial, state-of-the art, compact laser sources typically in the range of 10–200 mW, the detection sensitivity scales to minimum detectable absorption coefficients of 10^{-7} – $10^{-8} \text{ cm}^{-1} \text{ Hz}^{-1/2}$. This results in detection limits of sub-ppm to tens of ppb for the majority of trace gases of interest in atmospheric science, medical and industrial diagnostics. These limits are not as good as those which other sensitive spectroscopic methods such as cavity ring-down spectroscopy (CRDS) or integrated cavity output spectroscopy (ICOS) offer, typically values between 10^{-10} and $10^{-11} \text{ cm}^{-1} \text{ Hz}^{-1/2}$ using the same laser excitation powers. On the other hand, CRDS and ICOS require large cell volumes of tens to hundreds cubic centimeters compared to a QEPAS-based sensor platform, which can be as small as several cubic millimeters. A reduction of the PAS and QEPAS minimum detection limit would result in achieving optimum sensor performance—high detection sensitivity in cells of small volume. An alternative to increasing the microphone performance is to increase the power levels in the PAS or QEPAS cell. For example, a 15-fold increase in optical power of a fiber-coupled semiconductor DFB laser diode laser was achieved using an erbium-doped fiber amplifier [2]. This reduced the minimum detectable absorption coefficient to $9.5 \times 10^{-10} \text{ cm}^{-1} \text{ Hz}^{-1/2}$. However, this method has limited applicability, as fiber amplifiers are available only in a portion of the near-infrared wavelength range. A more universal method of achieving high power can be realized by placing a PAS cell into an optical resonant cavity. When the diode laser is mode-matched to the cavity and tuned into resonance with a fundamental optical mode of the cavity, the optical power inside the PAS cell P_c will exceed significantly the power incident onto the cavity from the laser P_i according to the Eq. (1)

$$P_c = P_i \frac{\eta T}{(1 - R)^2}, \quad (1)$$

where R and T represent, respectively, the reflectivity and transmission of the cavity mirrors and η is the coupling efficiency. Even a “modest” reflectivity of 99 % would allow a power enhancement of 100 times improving the PAS sensitivity to a level much closer to the other laser-based trace gas sensing techniques mentioned previously. With a cavity mirror reflectivity of 99.9–99.99 % PAS

would compare with CRDS or ICOS in detection sensitivity. In this case PAS would be able to take full advantage of its spectroscopic merits such as a small absorption cell volume and its “zero baseline” characteristic behavior. A recent experiment on cavity-enhanced PAS [10] demonstrated an expected 100-fold enhancement of the PAS signal with cavity mirrors of reflectivity $R = 99 \%$ with an external cavity diode laser (ECDL). The minimum detectable absorption was not evaluated in Ref. [10], but from the ratio of the strongest line in the upper plot of Fig. 3 in Ref. [10] to the peak-to-peak noise for 1-s averaging in the same figure, which is equal to 7.1 we can determine the noise-equivalent absorption. The absorption coefficient at the peak is $1.3 \times 10^{-5} \text{ cm}^{-1}$ which results in a noise-equivalent absorption of $1.9 \times 10^{-6} \text{ cm}^{-1} \text{ Hz}^{-1/2}$ that is \sim four orders of magnitude off the performance of CRDS or ICOS.

The main difficulty of a passive cavity enhancement technique similar to [10] is that the power enhancement in the cavity will cease as soon as the cavity resonance width becomes comparable to the laser line width due to the cavity finesse increasing with mirror reflectivity. By injecting a fraction of the laser radiation back into the cavity with the appropriate phase a significant reduction of the semiconductor laser line width and locking of the laser to the cavity can be achieved with corresponding orders of magnitude stronger power buildup [11]. This method known as “optical feedback locking” has been used in optical pumping experiments for more than two decades, with power enhancement factors as high as 10^5 readily achieved. The strong diode laser frequency pulling and the necessity of maintaining the phase of the optical radiation while the cavity resonance is being tuned by more than one cavity free spectral range (FSR) present a technical challenge in designing a robust self-sustaining system capable of spectral scanning and unattended, long-term operation, which may explain why an optical feedback-locking technique was not applied to PAS until recently.

A novel approach to the problem of robust locking and scanning was described in Ref [12]. A diode laser and cavity can be locked with a fast and robust electronic loop using one of the high-bandwidth locking methods known as Pound–Drever–Hall [13] or Hänsch–Couillaud [14] techniques. Robust locking is possible because a frequency-narrowed high intensity-laser beam inside a cavity results in an intense, low noise signal. A wavelength modulation at half of the acoustic resonance frequency of the intra-cavity PAS cell is applied to both the laser and the cavity while the laser is locked to the cavity. This yields a PAS signal at twice the modulation frequency, as is the case for wavelength-modulated PAS. This approach provides reliable scanning, but the system has a large background acoustic signal due to physical displacement of the cavity mirrors, a direct consequence

of the wavelength modulation of the cavity resonance. Recently, another method of reliable locking and scanning in optical power buildup cavity (OPBC) PAS was proposed in Ref [15], which does not require any additional optical components and high-frequency electronics and does not create acoustic background perturbations. A laboratory evaluation performed with near-infrared semiconductor DFB lasers demonstrated a detection sensitivity close to CRDS and ICOS. Hippler et al. [16] in their recent experiment on optical feedback-assisted PAS with a diode laser operating in the visible range and a linear cavity demonstrated the ability to perform spectral scans of more than one wavenumber using a frequency and phase-locking method similar to that of Ref. [15]. A minimum detectable absorption of $4.4 \times 10^{-9} \text{ cm}^{-1} \text{ Hz}^{-1/2}$ was reported in Ref. [16]. In order to avoid perturbations of the diode laser by back-reflection from the linear cavity front mirror it was necessary to use a combination of two Faraday isolators. Limited availability and high cost of high-performance Faraday isolators in the mid-infrared makes extension of their technique to the mid-infrared technically challenging. In this paper we report the application of the method described in Ref. [15] to the mid-infrared spectral region and demonstrate that the method is compatible with EC-QCL and offers the benefits of wide spectral scanning in combination with high sensitivity for multiple species analysis.

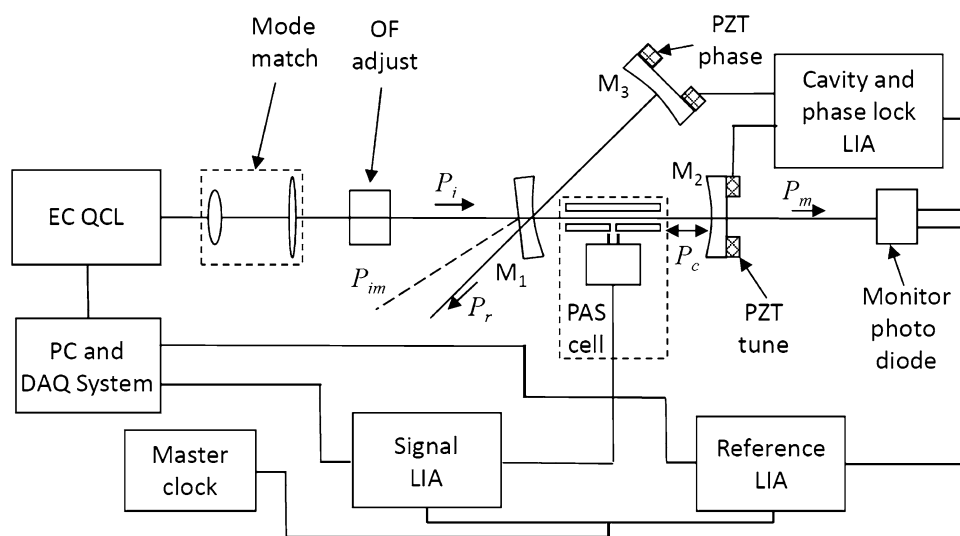
2 Experimental sensor platform and operation in the optical feedback regime

2.1 Spectrometer details

The experimental platform is shown in Fig. 1, based on Ref [15] with a $10.3 \mu\text{m}$ CW EC-QCL (DayLight Solutions,

model CW-MHF) that could be tuned without mode hops in a spectral range of 73 cm^{-1} , from 933 to $1,006 \text{ cm}^{-1}$, and a peak power of 72 mW at 970 cm^{-1} . This range is optimum for atmospheric ammonia detection and close to the emission wavelength of the CO_2 gas laser, which facilitates the commercial availability of required wavelength-dependent components, such as polarizers, wave plates and mirrors. The output beam of the EC-QCL is directed into a V-shaped buildup cavity formed by three mirrors, M_1 , M_2 , and M_3 through a mode-matching optical system composed of two spherical lenses. All three mirrors use ZnSe substrates (1 in. in diameter with 1 m radius of curvature; Los Gatos Research Inc., Mountain View, CA). The mirrors have an ultra-high reflectivity coating of 99.99 % with the reflectivity peak at $9.6 \mu\text{m}$ —quite far from the $10.4 \mu\text{m}$ wavelength where our EC-QCL operates. According to our measurements the transmission of the mirrors M_2 and M_3 operating at normal incidence is $T_2 = 0.057 \%$. Mirror M_1 operating at an angle of incidence of 23° has a slightly higher transmission of $T_1 = 0.091 \%$. The end mirrors M_2 and M_3 were mounted on 1-in. piezoelectric kinematic mirror mounts (KC1-PZ, Thorlabs, Newton, NJ) with a travel range of $7 \mu\text{m}$, which is sufficient to move the mirrors to ~ 1.5 cavity FSR at the operating wavelength of $10.4 \mu\text{m}$. The mirrors' translation range is larger than one cavity FSR, which is essential for operation in the optical feedback mode as described later on. The two arms of the cavity M_1M_2 and M_1M_3 were both equal to 100 mm which results in a fundamental mode diameter of 1.8 mm at the $1/e^2$ intensity level. We measured the beam profile of our EC-QCL and found it to have an elliptical cross section with the horizontal beam waist size $w_x = 1.25 \text{ mm}$, $M_x^2 = 1.17$ and vertical beam size $w_y = 1.03 \text{ mm}$ and $M_y^2 = 1.05$. This elliptical beam was relayed to the middle of the cavity arm M_1M_2 with a

Fig. 1 EC-QCL based OPBC-PAS trace gas sensor platform



combination of two spherical lenses with focal lengths of +75 mm and −50 mm. The magnification was chosen so that the mean value of the relayed ECDL horizontal beam waist and the vertical beam waist was equal to the cavity mode size. Thus, the ECDL beam was slightly mode mismatched in both directions. We observed some higher order mode excitation while scanning the EC-QCL, but the strongest higher order mode did not exceed several percent. The distance between the EC-QCL output mirror and the cavity mirror M_1 is 400 mm which corresponds to four times the cavity arm length. Simultaneous optical frequency tuning of the mutually locked cavity and EC-QCL was accomplished by the application of a tuning voltage to the PZT tuning element of the mirror M_2 , and a synchronous adjustment of the optical feedback phase by moving mirror M_3 in the opposite direction so as to keep the total cavity length constant. Furthermore, the cavity and EC-QCL were mounted on a vibration-isolated aluminum breadboard plate and placed in acoustically isolated Styrofoam box.

2.2 Resonant photo-acoustic cell

A custom-built resonant photo-acoustic cell was placed into the cavity between the mirrors M_1 and M_2 . A 42-mm-long stainless steel tube was used as an open-ended windowless acoustic resonator. An input aperture of miniature hearing aid microphone (EK3133, Knowles Electronics, LLC, Itasca, IL) was mounted in a small hole in the middle of the acoustic resonator tube. The insertion loss due to clipping of the intra-cavity beam by the tube with an inner diameter of 0.16 in. is $\sim 3.7 \times 10^{-5}$, which corresponds to 1.3 % of the total cavity roundtrip loss for four mirror reflections.

The PAS cell response as a function of frequency was determined using a wavelength-modulated 1,392 nm DFB laser with output power of 20.3 mW, which was tuned to the peak of an atmospheric water absorption line at 1,391.68 nm. The frequency dependence of the PAS cell response is shown in Fig. 2 by a blue line. The resonance frequency of the PAS cell was measured to be 3,986.6 Hz and the resonance width is 258 Hz at the level of $1/\sqrt{2}$ of the peak. Their ratio yields the Q-factor to be 15.5 for the PAS cell. The neperian absorbance of 0.142 at the peak of the same water line for a 91.4 cm path length was measured by conventional absorption spectroscopy. This gives an absorption coefficient of $1.55 \times 10^{-3} \text{ cm}^{-1}$ for this water line. The output voltage of the PAS cell at the line peak at $2f$ with an optimized wavelength modulation amplitude was 3.54 mV, which corresponds to PAS cell conversion coefficient $\eta = 113 \text{ V W}^{-1} \text{ cm}^{-1}$.

The noise floor was determined from averaged Fourier transformation of the digitized 1-s-long output voltage samples from the PAS cell located in the cavity with the

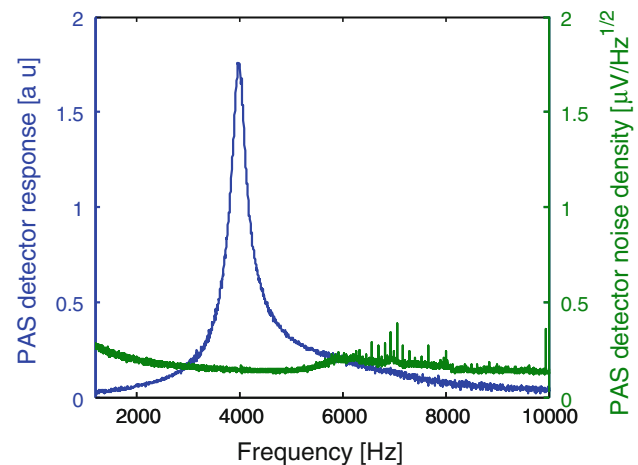


Fig. 2 Response curve and noise performance of the resonant PAS cell

acoustically isolated box in place but the intra-cavity beam blocked. The data were processed to obtain the cell output voltage noise spectral density as depicted in Fig. 2 by the green line. The measured voltage noise at the optimum detection frequency of 3,986.6 Hz was $0.145 \text{ } \mu\text{V Hz}^{-1/2}$. From this noise value and the PAS conversion coefficient measurement we determined the NNEA value of the normalized noise-equivalent absorption of the PAS cell to be $\sim 1.3 \times 10^{-9} \text{ cm}^{-1} \text{ W Hz}^{-1/2}$ —a value in agreement with the results reported by other groups, as discussed in Sect. 1.

2.3 Cavity and phase locking with optical feedback

The first OPBC applications were in optical pumping [11, 17]. The intra-cavity optical buildup power was approximately constant, and the locked laser frequency remained within the absorption line of the atom at all times. It was sufficient to adjust the length of the optical arm between the input mirror M_1 and the laser until the beam coming from the cavity had the same phase as the incident beam reflected from the laser resonator coupling mirror. The optical feedback would then result in locking the laser operation frequency to the cavity resonance. As soon as locking was achieved, the laser operation frequency will remain close to the cavity resonance peak even for large (hundreds of MHz) detuning of the intrinsic (unperturbed) laser diode frequency. In order to maintain static locking required for optical pumping, it was sufficient to keep the current of the laser within the locking range as well as to maintain the phase of the optical feedback by keeping the distance between the laser and the cavity constant using a piezoelectric transducer. The theory of a laser locked to a cavity by optical feedback is given in Ref. [20].

For photo-acoustic spectroscopy with the laser locked to OPBC by optical feedback a number of additional

conditions have to be achieved and maintained throughout the entire measurement. First of all, we need the optical power absorbed by the molecules of interest to be modulated under the condition that the laser should remain locked to the cavity mode regardless of the modulation. The next requirement is the ability of spectral scanning across a selected absorption line without disrupting optical feedback. Finally, the ability of self-recovery after a sudden disruption of the operation is important. The challenge of implementing these conditions is that the laser diode temperature and current alone no longer determine the operating wavelength because of the strong laser frequency pulling by the cavity. On the other hand, the cavity alone with its mirror mounted on a PZT also cannot be used as a wavelength reference. In this work, the amplitude modulation of the intra-cavity power due to periodic passages of the laser operating wavelength across the optical feedback resonance is used for simultaneous phase and frequency locking according to the method described in Ref. [15]. In the initial setup stage the optical feedback strength should be adjusted to ensure that the optical feedback-locking range does not exceed half of the frequency interval $\Delta\nu$ between the cavity modes.

The optical feedback strength adjustment was accomplished by a combination of a neutral density (ND) infrared filter (Edmund Optics, NT64-353) and a variable infrared ND filter with an optical density (OD) range from OD = 0 to OD = 1 (Reynard Corporation, R0231Z-10) inserted into the optical path between the cavity and the laser. A sufficiently large linear ramp to observe several cavity transmission peaks was applied to the laser current, and the optical feedback phase was adjusted to its optimum value. Subsequently, the variable ND filter transmission was adjusted until the areas of the zero transmitted intensity were equal to the width of the optical power buildup peaks. The required attenuation for achieving an optical feedback-locking range of \sim half of cavity $\Delta\nu = 1,500$ MHz was small, making it possible to use as much as 58 mW of the initial 70 mW EC-QCL power for the OPBC excitation. An explanation for the low required attenuation can be that an

EC-QCL is less sensitive to optical feedback because of its much smaller line width enhancement factor as compared to traditional diode lasers. The power losses can be further avoided either by replacing the linear attenuator between the V-shaped cavity and the laser by a partial Faraday isolator [21], or with a linear cavity by using a linear polarizer/quarter wave plate [17].

A symmetric sinusoidal wavelength modulation waveform was applied to the EC-QCL drive current of the EC-QCL, as shown by the dashed line in Fig. 3. The solid line in all three panels in this figure represents the intra-cavity buildup power calculated from the model described in Ref. [20]. The peak-to-peak value of the current modulation is adjusted to a value about twice as large as the optical feedback-locking range. The modulation frequency $f = 1,993.3$ Hz is one half of the PAS cell resonance frequency. When the optical feedback phase has its optimum value $\phi = 0$ the output voltage of the monitor photodetector, which is proportional to the intra-cavity power, will have a symmetrical shape, as shown in Fig. 3a. The output voltage of the photodetector is sent to the input of the lock-in amplifier (LIA) which is responsible for both cavity and phase locking. This cavity and phase-lock LIA operates at the fundamental wavelength modulation frequency f and has two outputs. The cavity and phase-lock LIA in-phase output voltage is a filtered product of its input voltage by a sinusoidal of frequency f , which is in phase with the wavelength modulation waveform. This waveform is depicted in Fig. 3 by the letter “s” and in red color. When the laser intrinsic optical frequency and the feedback phase both have values corresponding to perfect locking, the observed photodetector output voltage waveform is as shown in Fig. 3a. The average for one period of the product of the solid line waveform and the sinusoidal waveform will be equal to zero. This will also be the case for the filtered product that is sent to the cavity and phase-lock LIA in-phase output indicating a zero error signal of the laser frequency lock channel.

The quadrature cavity and phase-lock LIA output is the filtered product of its input voltage by a sinusoidal of frequency f , which is 90° out of phase with the wavelength

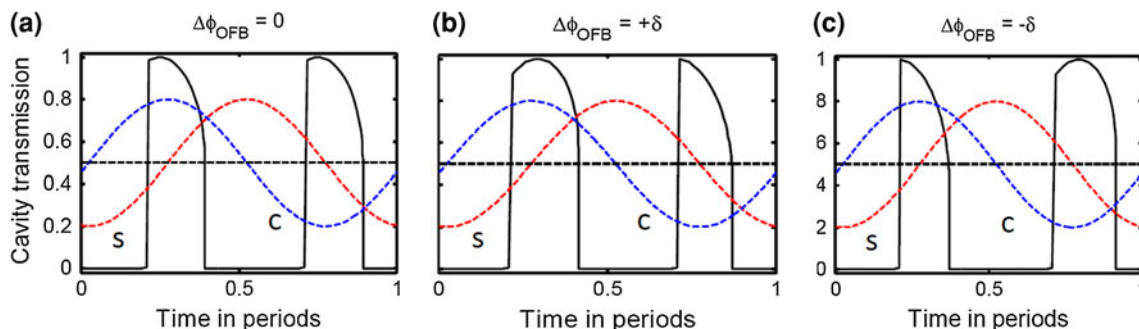


Fig. 3 Intra-cavity power waveforms in optical feedback phase and frequency locking

modulation waveform. This sinusoidal waveform is marked in Fig. 3 by the letter “c” and in blue color. The one period average of the product of the buildup power shown in Fig. 3a by a black solid line and the sinusoidal waveform “c” will also be equal to zero. This is because a positive half-period of the 90°-shifted sine in the first half of the period will cancel the product of the identical buildup waveform and a negative half-wave of the sinusoidal in the second half of the period. This results in a zero phase lock output voltage for an optical feedback phase error, $\phi = 0$.

In order to further explain the phase-lock operation let us assume that the intrinsic laser optical frequency maintains the correct value, but that the phase has drifted from its correct value, and thus a small phase error $\phi = -\delta$ occurs, as shown in Fig. 3b. The waveform loses its symmetry, and the cavity buildup intensity peak on the left side of the plot has a smaller area than the peak on the right side. The period average of the product has a negative value, indicating a phase-lock error. This error voltage is applied to the PZT phase, and the same signal will be applied as an increment of opposite sign to the PZT tuner. This in turn will restore the correct phase value without changing the cavity resonance frequency. Figure 3c depicts the case of a phase drift in a positive direction. Similarly, if we assume that the phase retains its value and the laser frequency shifts from its correct value, the two peaks in Fig. 3 will retain their shape but will move away from each other, thus generating a negative laser diode frequency error signal. This signal will be applied as an increment to the PZT tuner. This procedure will maintain the cavity resonance position in the middle of the wavelength modulation waveform both on its up-going and on the down-going segment. The experimental waveform of the monitor photodetector output voltage and the EC-QCL wavelength modulation waveform recorded by a digital oscilloscope and plotted in Fig. 4 which shows a close resemblance with our numerical model in Fig. 3a. This system provided

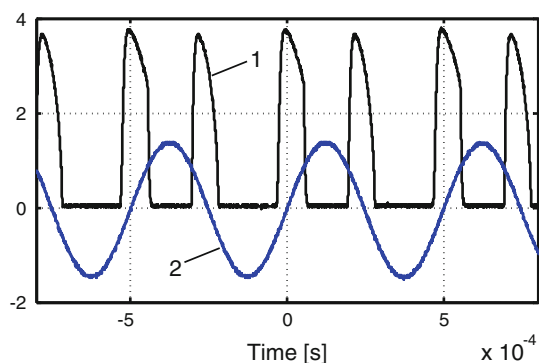


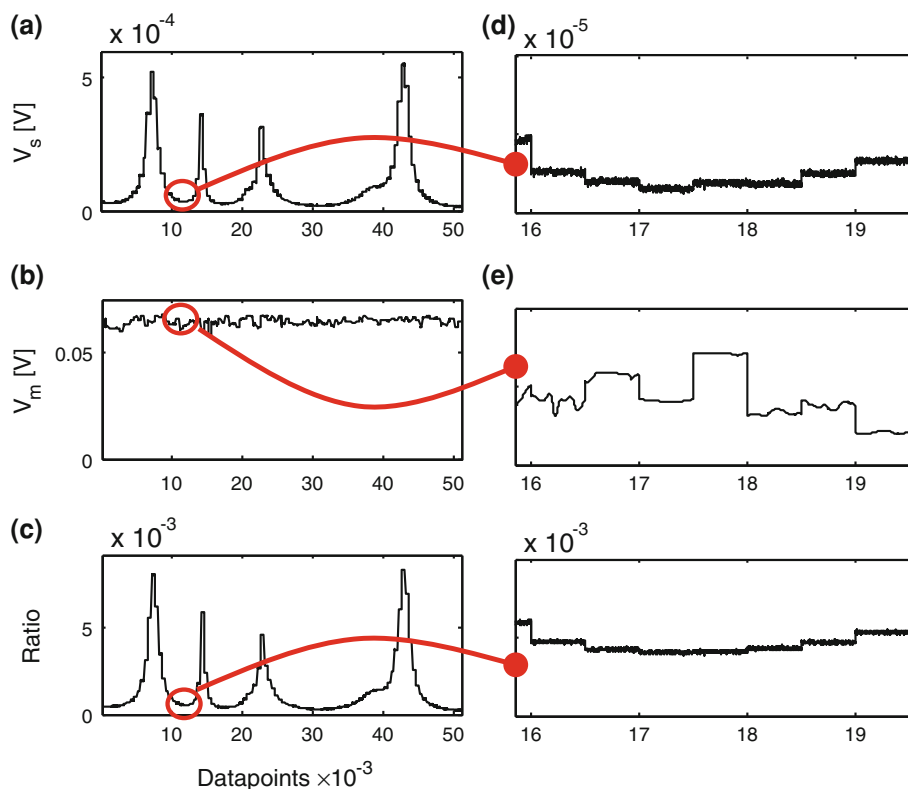
Fig. 4 Experimental waveforms in locked state. 1 monitor photodiode output voltage, 2 EC-QCL wavelength modulation waveform

robust locking of both the laser and the cavity, as well as maintaining the feedback phase for periods of up to tens of minutes.

2.4 Spectral scanning and data acquisition

Experimental data representing a 2.2-cm^{-1} wide EC-QCL scan, when the cavity mode is locked to the laser frequency and the optical feedback phase has its correct value, is shown in Fig. 5. The spectrum was recorded in a step mode which is one of the scanning regimes provided by the EC-QCL control module (Daylight Solutions, Inc). Computer control of the EC-QCL via GPIB interface initiated a scan to start at 960 cm^{-1} , remain at this wavenumber for 20 s, then move to the next spectral point, stay again 20 s, and repeat this sequence in increments of 0.02 cm^{-1} until the final wavenumber of 962.2 cm^{-1} is reached. The cavity lock system was set into a lock position when one of the cavity modes is locked to the laser and the optical feedback phase is at its optimum position. In order to maintain this lock at each scan step through the entire scan, the lock system increments the PZT voltage at each laser scan step. When the monotonically increasing PZT voltage reaches a predetermined threshold value close to its limit, the computer program resets the PZT voltage back towards its initial value in order to achieve a PZT displacement equal to one half of the operating wavelength. This reset displacement occurs on a time scale much shorter than the response time of the cavity lock system, which is therefore unable to detect such a fast displacement. The cavity lock system will sense when the next cavity mode is close to the laser operating frequency, and will re-lock to this mode. The cavity lock system can track small frequency increments of the EC-QCL until the PZT tuner approaches the end of its displacement range. In this manner the reset and relock sequence is repeated until the final scan wavenumber is reached. The optical feedback phase-locking system operates in exactly the same way thus permitting arbitrarily long seamless synchronous spectral scans of both the cavity and the EC-QCL. The plot in Fig. 5a) shows the filtered $2f$ output voltage of the PAS signal lock-in amplifier taken at a sampling frequency of $99,665\text{ Hz}$, which is 50 times the PAS cell resonance frequency. The stepwise character of this plot reflects the 20-s intervals between the scan steps. Figure 5b) shows the $2f$ output voltage of the second (monitor) lock-in amplifier sampled coherently with the signal lock-in amplifier and the same sampling frequency and sample clock. The digital filters of both lock-in amplifiers have exactly the same settings, a time constant of 0.3 s and a slope of 24 dB/oct . The equivalent noise bandwidth of both channels is 0.26 Hz . The steep digital filter slope helped to suppress some residual spurious power line interference that is visible on the PAS detector

Fig. 5 Cavity-enhanced PAS scan of laboratory air at ambient pressure



noise power spectral density plot at frequencies between 6 and 8 kHz in Fig. 2. This coherent sampling of the PAS signal and of the monitor photodetector signal is important for two reasons [15]. One reason is that the laser power fluctuations are filtered out. The second reason is that it permits the normalization of the PAS signal to only that part of the intra-cavity optical power that is effective in enhancing the PAS cell response and thus provide immunity of the measurement results to various drifts, such as laser-to-cavity coupling efficiency drift, the buildup power decrease due to mirror contamination and the possible loss of laser output power with time. Ideally, the intra-cavity buildup optical power peaks during the laser frequency scan should have a shape similar to Fig. 3a with some gradual change of the amplitude peaks that follows EC-QCL output power variations within the spectral tuning range. The buildup peaks may be different from the ideal case as can be seen in Fig. 4. The reasons for this may be imperfections of the feedback loop operation and external perturbations. As a result, the Fourier component of the buildup power (i.e., the monitor lock-in output V_m) at $2f$, plotted in Fig. 5b has variations of several percent at one laser scan point and between scan points. Even if the total laser power remains constant, its contribution to the PAS signal excitation may vary when the shape or position of the buildup peaks changes (see magnified part of the scan in the right panel of Fig 5). This plot represents a residual absorption between two overlapped spectral lines, which

should look like a broad smooth minimum. However, the PAS signal depicted in Fig. 5d shows variation that reflects the effective buildup power deviations visible in Fig. 5e. This figure shows excursions of the effective buildup power as large as $\sim 10\%$ peak to peak regardless that the EC-QCL power is stable in a scan. We can see these variations to cancel out in the ratio of the two signals depicted in Fig. 5f. The impact of the PAS signal excitation efficiency variations can thus be eliminated. Benefits of the normalization of the PAS transducer signal to the effective intra-cavity power make PAS measurements not sensitive to optical misalignment and aging of the cavity mirrors and laser. Once the conversion coefficient between optical absorbance and the value of the normalized PAS signal has been determined with a sample gas as a part of the instrument initial setup, it can be used in subsequent measurements for determining directly the absorbance and calculating the target molecule concentration.

2.5 Analysis of resonance enhancement and sensitivity

In our evaluation of the EC-QCL-based OPBC-PAS gas sensor platform, we used the absorption of water vapor present in laboratory air. Hence, we could not use a reference sample approach for the spectrometer calibration. Instead the direct absorption of the atmospheric water absorption line was measured at 1,391.68 nm with a near-IR DFB laser as described in Sect. 2.2. This open path near-

infrared measurement made at the same time as a cavity-enhanced PAS scan, and spectral fit with HITRAN 2008 database [18] for our experimental conditions yielded a water vapor concentration of 1.1 % at 21.2 °C and atmospheric pressure of 101 kPa. The absorption spectrum of air for the spectral range of the EC-QCL scan using data from HITRAN 2008 database, and the scaled averaged ratio data of Fig. 5c were used to achieve the best match with the HITRAN absorption spectrum. The result is shown in Fig. 6. Each of the experimental datapoints shown in Fig. 6 as circles represents a 20 s average of all normalized data for each EC-QCL wavenumber step. The solid line is the atmospheric absorption calculated from HITRAN. The absorption line at $\sim 960.5 \text{ cm}^{-1}$ has an absorption coefficient of $0.70 \times 10^{-6} \text{ cm}^{-1}$, which corresponds to a PAS cell signal of 0.53 mV (shown in Fig. 5a). In Sect. 2.2 we reported a PAS cell noise density of $0.145 \mu\text{V Hz}^{-1/2}$. We could achieve a very good match between the measured points and HITRAN data by simple scaling of the experimental values with no shift required. This allows us to assume that the photo-acoustic background signals and their contributions to the baseline noise is negligible, and that we can use the measured value of the PAS cell noise density for the spectrometer sensitivity evaluation. The signal-to-noise ratio for the indicated absorption line per unit bandwidth is $3.7 \times 10^{-3} \text{ Hz}^{-1/2}$, which yields a noise-equivalent absorption of $1.9 \times 10^{-10} \text{ cm}^{-1} \text{ Hz}^{-1/2}$. Hence the detection sensitivity of OPBC-enhanced PAS is comparable to the most sensitive laser-based spectroscopic sensor techniques reported in the literature [1]. The EC-QCL power available in this experiment is 56 mW which results in a NNEA for OPBC-PAS $1.1 \times 10^{-11} \text{ cm}^{-1} \text{ W Hz}^{-1/2}$. It is also interesting to compare the sensitivity of our cavity-enhanced PAS instrument with conventional PAS. For example, if we

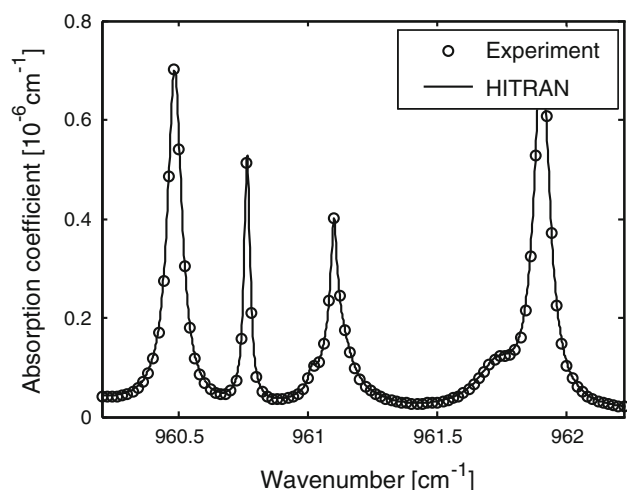


Fig. 6 PAS spectrum comparison with HITRAN 2008

assume that our PAS cell is used directly without the cavity, then with the available optical power of 56 mW a noise-equivalent absorption of $2.3 \times 10^{-8} \text{ cm}^{-1} \text{ Hz}^{-1/2}$ could be obtained thus gaining a factor of 121 times in detection sensitivity. A direct comparison would be even more valuable, and the selected absorption line would be measurable with the NNEA based on conventional PAS sensor technology. However, it was not feasible to make a direct comparison with the available EC-QCL because it does not allow wavelength modulation at a frequency of 1,993 kHz with an amplitude that WMS requires at the atmospheric pressure. The EC-QCL wavelength modulation mode available from the EC-QCL controller module does not allow modulation frequencies higher than 100 Hz by application of a sinusoidal voltage to the PZT built into the EC-QCL control module. The second wavelength modulation mode via the QCL current input has a modulation depth limited to 2.5 GHz, whereas conventional WMS of the water vapor lines requires $\sim 7.5 \text{ GHz}$. It was feasible to operate the OPBC as it required a peak-to-peak laser frequency excursion of only 0.6 GHz. An alternative approach of OPBC gain evaluation is to compare the intra-cavity power with initial power. For evaluation of the intra-cavity power the EC-QCL is tuned to the minimum atmospheric absorption at $\sim 961.45 \text{ cm}^{-1}$. This allows a measurement of the optical power P_m transmitted by the cavity mirror M_2 (see Fig. 1), the power P_r reflected from the cavity mirror M_1 and the power P_i incident onto the three mirror OPBC. The incident power was sampled by measuring a reflection P_{im} from the mirror substrate front surface shown in the Fig. 1 by a dashed line. From a measured value of $P_m = 2.6 \text{ mW}$ transmitted by one of the OPBC end mirrors the power inside the cavity, P_{Cirq} can be determined to be $P_{\text{Cirq}} = P_m/T_2 = 4.8 \text{ W}$. This value can be confirmed by comparing the incident power $P_i = 56 \text{ mW}$ with the power $P_r = 29 \text{ mW}$ reflected from the cavity at the power buildup peak. Between the peaks with no buildup most of the incident radiation will be reflected from the cavity mirror M_1 which results in an optical power $P_i \times R_1 \approx 56 \text{ mW}$. At the buildup maximum the beam reflected from M_1 will destructively interfere with a fraction of the circulating power $P_1 = P_{\text{Cirq}} \times T_1 = 4.3 \text{ mW}$ transmitted by the same mirror to yield P_r . Indeed $(\sqrt{P_i \times R_1} - \sqrt{P_1})^{1/2}$ results in a value of $\sim 29 \text{ mW}$. The power coupled into the cavity at the buildup peak was $P_i - P_r = 27 \text{ mW}$ which is \sim half of the available EC-QCL power. The circulating OPBC laser beam will traverse the PAS cell twice in one roundtrip which makes its effective power twice as large as the circulating power. The effective intra-OPBC power, P_{Cirq} of 9.6 W is 181 times higher than the total available EC-QCL power. Therefore, the same gain in sensitivity can be expected. However, our estimate based on the generated

PAS signal and PAS cell noise properties in the previous paragraph yielded an OPBC gain value that is ~ 1.5 times lower. Therefore, in our evaluation of OPBC-enhanced PAS not all of available P_{Circ} of 9.6 W was effective in PAS signal generation. An explanation for the lower efficiency of PAS signal excitation can be found by comparing the intra-cavity power waveforms shown in Figs. 3 and 4 depicting different WMS modulation waveforms. The highest PAS signal excitation efficiency can be achieved for a rectangular excitation power waveform with a duty factor close to 50 %, as in conventional amplitude-modulated PAS. Our calibration value for PAS response in Sect. 2.2 was obtained by WMS for a Lorentzian absorption line with an optimum modulation index of 2.2 times the absorption line width. This form of modulation is about 1.46 times less efficient than rectangular amplitude modulation. The OPBC waveform in an ideal case, as depicted in Fig. 3a, has a shape closer to a rectangular modulation. Therefore, the PAS signal excitation in an OPBC can be nearly as efficient as with rectangular modulation by making the OPBC waveform duty factor ~ 50 %. The actual intra-cavity buildup power waveform shown by a black trace in Fig. 4 has a duty factor of <50 % which explains the lower sensitivity gain.

3 Conclusions

A mid-infrared photo-acoustic spectrometer using a 10.4- μm EC-QCL and an OPBC composed of high reflectivity dielectric mirrors capable of high trace gas detection sensitivity is reported. The V-shaped cavity configuration resulted in efficient injection of the quantum cascade laser radiation into the OPBC using only a minimum number of optical elements. The EC-QCL power is increased 181 times by an OPBC-PAS sensor configuration which resulted in a 121-fold reduction of the NNEA as compared to a conventional PAS sensor architecture. The capability of automatically maintaining a lock of the laser to the cavity frequency and an optical feedback phase lock during wavelength scanning of the EC-QCL was demonstrated. A novel method of normalization of the intra-cavity PAS cell signal to monitor the photodetector signal at the same detection harmonics was evaluated. This normalization method makes the PAS spectrometer response independent of optical alignment drifts and cavity mirror contamination. The reported PAS spectrometer operation principle based on optical feedback is applicable to different types of infrared-tunable semiconductor lasers such as traditional semiconductor diode lasers, quantum cascade lasers and interband cascade lasers as well as external cavity-QCLs or ICLs. For example, using conventional PAS a NNEA of $1.9 \times 10^{-10} \text{ cm}^{-1} \text{ Hz}^{-1/2}$ was demonstrated, which offers

detection limits lower than 10 ppbv. As an example, ammonia was monitored in urban air using conventional PAS with a limit of detection of 8 ppbv [19]. With OPBC-enhanced PAS, we expect to obtain a minimum detectable concentration of <10 pptv for the same ammonia rotational–vibrational absorption line located at 965.35 cm^{-1} .

Acknowledgments The Rice University group acknowledges financial support from a National Science Foundation (NSF) grant EEC-0540832 entitled “Mid-InfraRed Technologies for Health and the Environment (MIRTHE)”, and grant C-0586 from the Robert Welch Foundation.

References

1. R.F. Curl, F. Capasso, C. Gmachl, A.A. Kosterev, B. McManus, R. Lewicki, M. Pushkarsky, G. Wysocki, F.K. Tittel, Quantum cascade lasers in chemical physics. *Chem. Phys. Lett.* **487**, 1–18 (2010)
2. M.E. Webber, M. Pushkarsky, C.K.N. Patel, Fiber-amplifier-enhanced photoacoustic spectroscopy with near-infrared tunable diode lasers. *Appl. Opt.* **42**, 2119–2126 (2003)
3. A. Miklos, P. Hess, Z. Bozoki, Application of acoustic resonators in photoacoustic trace gas analysis and metrology. *Rev. Sci. Instrum.* **72**, 1937–1955 (2001)
4. V.A. Kapitanov, Y.N. Ponomarev, High resolution ethylene absorption spectrum between 6035 and 6210 cm^{-1} . *Appl. Phys. B Lasers Opt.* **90**, 235–241 (2008)
5. L.B. Kreuzer, Ultralow gas concentration infrared absorption spectroscopy. *J. Appl. Phys.* **42**, 2934–2943 (1971)
6. S.C. Thompson, J.L. Lopresti, E.M. Ring, H.G. Nepomuceno, J.J. Beard, W.J. Ballard, E.V. Carlson, Noise in miniature microphones. *J. Acoust. Soc. Am.* **111**, 861–866 (2002)
7. T. Laurila, H. Cattaneo, V. Koskinen, J. Kauppinen, R. Hernberg, Diode laser-based photoacoustic spectroscopy with interferometrically-enhanced cantilever detection. *Opt. Express* **13**, 2453–2458 (2005)
8. A.A. Kosterev, F.K. Tittel, D.V. Serebryakov, A.L. Malinovsky, I.V. Morozov, Applications of quartz tuning forks in spectroscopic gas sensing. *Rev. Sci. Instrum.* **76**, 043105 (2005)
9. A.A. Kosterev, P.R. Buerki, L. Dong, M. Reed, T. Day, F.K. Tittel, QEPAS detector for rapid spectral measurements. *Appl. Phys. B* **100**, 173–180 (2010)
10. A. Rossi, R. Buffa, M. Scotoni, D. Bassi, S. Iannotta, A. Boschetti, Optical enhancement of diode laser-photoacoustic trace gas detection by means of external Fabry–Perot cavity. *Appl. Phys. Lett.* **87**, 041110 (2005)
11. B. Dahmani, L. Hollberg, R. Drullinger, Frequency stabilization of semiconductor lasers by resonant optical feedback. *Opt. Lett.* **12**, 876–878 (1987)
12. M. Selker, A. Riddle, B. Paldus, System and method for gas analysis using doubly resonant photoacoustic spectroscopy. USA Patent 7263871 (2005)
13. J. Ye, L.-S. Ma, J. Hall, Ultrasensitive detections in atomic and molecular physics: demonstration in molecular overtone spectroscopy. *JOSA B* **15**, 6–15 (1998)
14. T.W. Hansch, B. Couillaud, Laser frequency stabilization by polarization spectroscopy of a reflecting reference cavity. *Opt. Commun.* **35**, 441–444 (1980)
15. A. Kachanov, S. Koulikov, Method and apparatus for the photoacoustic identification and quantification of analyte species in a gaseous or liquid medium. USA Patent application 2011/0214479, 2 March (2010)

16. M. Hippler, C. Mohr, K.A. Keen, E.D. McNaghten, Cavity-enhanced resonant photoacoustic spectroscopy with optical feedback cw diode lasers: A novel technique for ultratrace gas analysis and high-resolution spectroscopy. *J. Chem. Phys.* **133**, 044308 (2010)
17. C.E. Tanner, B.P. Masteron, C.E. Wieman, Atomic beam collimation using a laser diode with a self-locking power buildup cavity. *Opt. Lett.* **13**, 357–359 (1988)
18. L.S. Rothman et al., The HITRAN 2008 molecular spectroscopic database. *JQSRT* **110**, 533–572 (2009)
19. L. Gong, R. Lewicki, R.J. Griffin, J.H. Flynn, B.L. Lefer, F.K. Tittel, Atmospheric ammonia measurements in Houston TX using an external-cavity quantum cascade laser-based sensor. *Atmos. Chem. Phys.* **11**, 9721–9733 (2011)
20. Ph Laurent, A. Clairon, Ch. Bréant, Frequency noise analysis of optically self-locked diode lasers. *IEEE J. Quant. Electron.* **25**, 1131–1142 (1989)
21. J. Morville, M. Chenevier, A.A. Kachanov, D. Romanini, Trace detection with DFB lasers and cavity ring-down spectroscopy. *Proc. SPIE* **4485**, 236–243 (2002)